Transport of Charged Macromolecules in an Electric Field by a Numerical Method. 1. Application to a Sphere

Stuart A. Allison* and P. Nambi

Department of Chemistry, Georgia State University, Atlanta, Georgia 30303

Received February 11, 1992; Revised Manuscript Received April 16, 1992

ABSTRACT: The discretized integral equation (DIE) method by Youngren and Acrivos (*J. Fluid Mech.* **1975**, *69*, 377) is generalized to include the effect of time-independent external forces on the transport of rigid macromolecules undergoing Stokes flow in an incompressible, unbounded fluid. According to Ladyzhenskaya (*The Mathematical Theory of Viscous Incompressible Flow*; Gordon and Breach: New York, 1963), this is achieved by adding additional terms to the integral equations for the fluid pressure and velocity fields in the vicinity of the macromolecule. The generalized DIE method should be useful in modeling electrophoresis and related electrokinetic phenomenon of charged polyions in solution. To verify the method, it is applied to an insulating charged sphere subjected to a constant external electric field in which relaxation of the ion atmosphere from its equilibrium distribution is ignored. Numerical solutions of the electrophoretic mobility as well as pressure and velocity fields around the polyion are in good agreement with the predictions of Henry (*Proc. R. Soc. London*, **1931**, *A133*, 106).

Introduction

In the past 25 years, two distinct numerical methods have been developed and applied successfully to the transport of rigid macromolecules undergoing Stokes flow in an incompressible, unbounded fluid. The most extensively used method involves bead or "shell" models in which the macromolecule is represented as an arbitrary array of beads whose size and shape resembles the actual macromolecule as closely as possible.[1-6] In the integral equation approach,[7-9] the fundamental singular solutions of the linearized Navier–Stokes and solvent incompressibility equations are continuously distributed over the surface of the particle and, in the general case, the surrounding media as well. The boundary conditions on the solvent at the particle surface and at great distances from it then lead to integral equations for the surface stress forces and also external forces acting on the fluid. Youngren and Acrivos implemented this approach numerically by reducing the integral equations to a linear system of algebraic equations.[8] Both the discretized integral equation (hereafter referred to as DIE) and shell model approaches are conceptually quite similar to each other. Basically, one views the hydrodynamic properties of the macromolecule as resulting from the solvent perturbation by point sources of friction uniformly distributed over the object's surface. In ths shell model, the sources of friction are beads whereas in the DIE algorithm of Youngren and Acrivos they are a series of small platelets which cover the macromolecule. In either case, it appears that either model yields exact transport coefficients for arbitrary rigid bodies in the limit of a large number of beads or platelets.

Both the bead and DIE (as implemented in refs 8 and 9) methods are deficient in the respect that external forces on the solvent are ignored. For charged macromolecules, this neglect is significant since electrostatic forces on the co-ion and counterion atmospheres result in net external forces on the surrounding fluid. These forces alter the pressure and velocity fields around the particle and hence its transport properties. One well-known consequence is the osmotic pressure around a stationary charged sphere.[10] External forces are important in the transport of polyions in external electric fields (electrophoresis), flow processes which alter the distribution of the ion atmosphere from its equilibrium state (electrosedimentation and electroviscosity), and related electrokinetic phenomenon.[11] Since the pioneering study of von Smoluchowski,[12] a great deal of work has been done on the theory of electrophoresis. The charged sphere has been extensively studied by Henry,[13] Overbeek,[14] Booth,[15] Wiersema and co-workers,[16] O'Brien, White, and co-workers,[17-19] and others. This particular problem has proven to be difficult, but mathematically tractable. Relating the electrophoretic mobility of spherical charged colloidal particles to surface or ζ potentials has provided the motivation for its study. In the linear response regime and for steady-state external fields, it appears that the spherical particle (with centrosymmetric charge distribution) has now been solved rigorously. (By "rigorous" we mean a solution of the continuum model for the fluid (Navier–Stokes and solvent incompressibility), charge distribution (Poisson), and ion transport equations.) Cylinders[13,20] have also been studied, by the solutions remain approximate.[11] In addition, the formalisms of Fixman[21,22] and Dukhin and co-workers[23,24] should also be cited. Except for a sphere or polyion whose ion atmosphere is thin relative to the linear dimension of the particle, the steady-state transport properties remain largely undetermined. The current state of affairs with regard to the transport of charged macromolecules is analogous to that of uncharged particles before the advent of bead or DIE methods.

The motivation of the present study has been the development of a numerical method which incorporates the effects of steady-state external forces on the solvent. It is not at all transparent to us how to generalize the bead method. The integral equation approach, on the other hand, can be generalized to acheive this end. In fact, the fundamental "master equations" were given by Ladyzhenskaya[7] almost 30 years ago. The presence of external forces basically contributes additional terms to the integral equations for the pressure and fluid velocity fields. Thus, their inclusion involves a straightforward extension of the DIE approach developed by Youngren and Acrivos.[8]

The objectives of this work are 2-fold: first, develop a generalization of the DIE method to include external forces and, second, show that it is a viable method by considering test cases. The test cases we shall consider are the transport of charged spherical particles at several different ζ potentials. To simplify matters further, relaxation of

* Corresponding author.

0024-9297/92/2225-3971$03.00/0

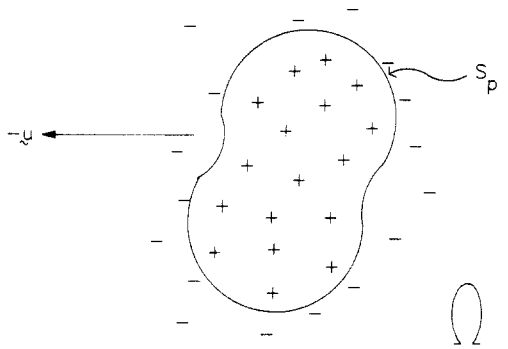

Figure 1. Schematic of a polyion translating with velocity $-\mathbf{u}$ in an aqueous fluid which is at rest far from the surface S_p. Ω denotes the volume of fluid external to the polyion.

the ion atmosphere shall also be ignored in this initial study. This problem was thoroughly investigated by Henry,[13] and the DIE results carried out here shall be tested using his equations. In addition to electrophoretic mobilities, a comparison of actual fluid pressure and velocities around the polyion shall also be presented.

Integral Equations

In this work we shall use the convention of representing vector quantities with bold lower case letters and tensor quantities with bold upper case letters. Consider an arbitrary rigid particle moving through an unbounded incompressible fluid with velocity $-\mathbf{u}(\mathbf{x})$. Far from the particle, the fluid velocity, $\mathbf{v}(\mathbf{x})$, is taken to vanish. Stick boundary conditions shall be assumed, which means $\mathbf{v}(\mathbf{x}) = -\mathbf{u}(\mathbf{x})$ at the polyion surface. Rotation is ignored in the present study. Its inclusion would require different boundary conditions on the fluid velocity at the polyion surface. Let Ω denote the unbounded domain of the fluid and S_p the surface which encloses the polyion. A schematic is shown in Figure 1. At low Reynolds number, the Navier–Stokes and solvent incompressibility equations can be written[25]

$$\eta\nabla^2\mathbf{v}(\mathbf{x}) - \nabla p(\mathbf{x}) = -\mathbf{s}(\mathbf{x}) \qquad \mathbf{x} \in \Omega \tag{1}$$

$$\nabla\cdot\mathbf{v}(\mathbf{x}) = 0 \tag{2}$$

where η is the solvent viscosity, $p(\mathbf{x})$ is the pressure and $\mathbf{s}(\mathbf{x})$ is the force per unit volume on the fluid at $\mathbf{x}$ due to external forces. Also, ∇^2, ∇, $\nabla\cdot$ refer to Laplacian, gradient, and divergence, respectively. In this work, we are interested in the transport of polyions and their accompanying ion atmospheres for which

$$\mathbf{s}(\mathbf{x}) = -\rho(\mathbf{x})\nabla\Lambda(\mathbf{x}) \tag{3}$$

where ρ is the charge density and Λ the electrostatic potential. According to Ladyzhenskaya,[7] the unique solution of $\mathbf{v}$ and p can be written in terms of integral equations. Before writing these out, it will be helpful to consider the fundamental singular solutions of the linearized Navier–Stokes system ($(\mathbf{U})_{ij}$ and $\mathbf{q}_i$ vanish as $|\mathbf{x}| \to \infty$)

$$\eta\nabla^2(\mathbf{U}(\mathbf{x},\mathbf{y})\cdot\mathbf{e}_k) - \nabla(\mathbf{q}(\mathbf{x},\mathbf{y})\cdot\mathbf{e}_k) = \delta(\mathbf{x}-\mathbf{y})\mathbf{e}_k \tag{4}$$

$$\nabla\cdot(\mathbf{U}(\mathbf{x},\mathbf{y})\cdot\mathbf{e}_k) = 0 \tag{5}$$

where $\mathbf{e}_k$ is a unit vector in the k direction, δ denotes the delta function, and all differential operators act on the field variable $\mathbf{x}$ rather than the source variable $\mathbf{y}$. The solutions are[7,8]

$$\mathbf{U}(\mathbf{x},\mathbf{y}) = -\frac{1}{8\pi\eta r}[\mathbf{I} + \mathbf{R}(\mathbf{x},\mathbf{y})] \tag{6}$$

$$\mathbf{q}(\mathbf{x},\mathbf{y}) = -\frac{1}{4\pi r^3}\mathbf{r} \tag{7}$$

where $\mathbf{r} = \mathbf{x} - \mathbf{y}$, $r = |\mathbf{r}|$, $\mathbf{I}$ is the 3×3 identity matrix, and

$$(\mathbf{R})_{ij} = \mathbf{e}_i\cdot\mathbf{R}\cdot\mathbf{e}_j = r_i r_j/r^2 \tag{8}$$

In terms of the singular solutions, $\mathbf{v}$ and $\mathbf{p}$ are given by

$$\mathbf{v}(\mathbf{x}) = \mathbf{v}^{(0)}(\mathbf{x}) + \mathbf{v}^{(1)}(\mathbf{x}) + \mathbf{v}^{(2)}(\mathbf{x}) \tag{9}$$

$$p(\mathbf{x}) = p^{(0)}(\mathbf{x}) + p^{(1)}(\mathbf{x}) + p^{(2)}(\mathbf{x}) \tag{10}$$

where

$$\mathbf{v}^{(0)}(\mathbf{x}) = -\int\int\int_\Omega \mathbf{U}(\mathbf{x},\mathbf{y})\cdot\mathbf{s}(\mathbf{y})\, d^3\mathbf{y} \tag{11}$$

$$p^{(0)}(\mathbf{x}) = -\int\int\int_\Omega \mathbf{q}(\mathbf{x},\mathbf{y})\cdot\mathbf{s}(\mathbf{y})\, d^3\mathbf{y} \tag{12}$$

$$\mathbf{v}^{(1)}(\mathbf{x}) = -\int\int_{S_p} \mathbf{U}(\mathbf{x},\mathbf{y})\cdot\mathbf{f}(\mathbf{y})\, dS_y \tag{13}$$

$$p^{(1)}(\mathbf{x}) = -\int\int_{S_p} \mathbf{q}(\mathbf{x},\mathbf{y})\cdot\mathbf{f}(\mathbf{y})\, dS_y \tag{14}$$

$$\mathbf{v}^{(2)}(\mathbf{x}) = -\frac{3}{4\pi}\int\int_{S_p} r^{-3}\mathbf{r}(\mathbf{v}(\mathbf{y})\cdot\mathbf{R}(\mathbf{x},\mathbf{y})\cdot\mathbf{n}(\mathbf{y}))\, dS_y \tag{15}$$

$$p^{(2)}(\mathbf{x}) = \frac{\eta}{2\pi}\int\int_{S_p} r^{-3}\mathbf{v}(\mathbf{y})\cdot[\mathbf{I} - 3\mathbf{R}(\mathbf{x},\mathbf{y})]\cdot\mathbf{n}(\mathbf{y})\, dS_y \tag{16}$$

In eqs 13 and 14, $\mathbf{f}(\mathbf{y})$ is the stress force per unit area on the fluid due to the particle at position $\mathbf{y}$ on the particle surface and dS_y denotes surface integration over the enclosing particle surface S_p. In eqs 15 and 16, $\mathbf{n}(\mathbf{y})$ denotes the *inward* unit normal to the particle surface at Y. The stress forces are related to the stress tensor, $\mathbf{T}$, by

$$\mathbf{f}(\mathbf{y}) = (\lim_{\mathbf{x}\to\mathbf{y}} \mathbf{T}(\mathbf{x}))\cdot\mathbf{n}(\mathbf{y}) \tag{17}$$

where

$$T_{ij}(\mathbf{x}) = -p(\mathbf{x})\delta_{ij} + \eta\left(\frac{\partial v_i(\mathbf{x})}{\partial x_j} + \frac{\partial v_j(\mathbf{x})}{\partial x_i}\right) \tag{18}$$

Since the velocity and pressure fields are unknown, so are the forces $\mathbf{f}(\mathbf{y})$. As shown below, however, they can be determined by solving for $\mathbf{v}(\mathbf{x})$ at the particle surface which is known from the boundary conditions. Equations 9–16 are a generalization of Youngren and Acrivos[8] who considered the case of no external fluid forces ($\mathbf{s}(\mathbf{y}) = 0$). Thus, the $\mathbf{v}^{(0)}$ and $p^{(0)}$ terms are missing in their work.

Some caution must be used in applying these equations to the polyion surface since $\mathbf{v}^{(2)}(\mathbf{x})$ and $p^{(1)}(\mathbf{x})$ undergo a discontinuous jump at S_p.[7,8] Specifically

$$\lim_{\mathbf{x}\to\mathbf{x}_0} \mathbf{v}^{(2)}(\mathbf{x}) = \mathbf{v}^{(2)}(\mathbf{x}_0) + \frac{1}{2}\mathbf{v}(\mathbf{x}_0) \tag{19}$$

where $\mathbf{x} \in \Omega$ but not S_p and $\mathbf{x}_0 \in S_p$. Combining this with the boundary condition $\mathbf{v}(\mathbf{x}_0) = -\mathbf{u}(\mathbf{x}_0)$, we arrive at

$$-\mathbf{u}(\mathbf{x}_0) = 2(\mathbf{v}^{(0)}(\mathbf{x}_0) + \mathbf{v}^{(1)}(\mathbf{x}_0) + \mathbf{v}^{(2)}(\mathbf{x}_0)) \tag{20}$$

In the case of pure translation where $\mathbf{u}(\mathbf{x}_0)$ is constant over the particle surface (as depicted in Figure 1) for an

arbitrary polyion, it has been shown that[7]

$$\mathbf{v}^{(2)}(\mathbf{x}_0) = -\frac{1}{2}\mathbf{u} \tag{21}$$

where the field dependence of $\mathbf{u}$ has been dropped. Equation 20 simplifies to

$$-\mathbf{u} = \frac{1}{8\pi\eta}\int\int\int_{\Omega} r_0^{-1}[\mathbf{I} + \mathbf{R}(\mathbf{x}_0,\mathbf{y})]\cdot\mathbf{s}(\mathbf{y})\, d^3\mathbf{y} + \frac{1}{8\pi\eta}\int\int_{S_p} r_0^{-1}[\mathbf{I} + \mathbf{R}(\mathbf{x}_0,\mathbf{y})]\cdot\mathbf{f}(\mathbf{y})\, dS_y \tag{22}$$

Following Youngren and Acrivos,[8] the surface of the polyion is broken up into N smaller surfaces or patches, and the assumption is made that the stress forces, $\mathbf{f}(\mathbf{y})$, are constant over the patch to a good approximation. When external forces are present, it is also necessary to subdivide the space surrounding the particle into volume elements as well. For the problems of interest in this work, external forces will only be significant near the charged particle so that the unbounded domain, Ω, can be replaced with a much smaller bounded one to a good approximation. As before, the assumption is made that $\mathbf{s}(\mathbf{y})$ is essentially constant over the volume element. Let there be M volume elements labeled $N + 1$ to $N + M$ (the first N labels referring to surface elements) so that eq 2 can be written

$$-\mathbf{u} = \sum_{j=1}^{N}\mathbf{C}_j(\mathbf{x}_0)\cdot\mathbf{f}_j + \sum_{j=N+1}^{N+M}\mathbf{B}_j(\mathbf{x}_0)\cdot\mathbf{s}_j \tag{23}$$

where

$$\mathbf{B}_j(\mathbf{x}_0) = \frac{1}{8\pi\eta}\int\int\int_{V_j} r_0^{-1}[\mathbf{I} + \mathbf{R}(\mathbf{x}_0,\mathbf{y})]\, d^3\mathbf{y} \tag{24}$$

$$\mathbf{C}_j(\mathbf{x}_0) = \frac{1}{8\pi\eta}\int\int_{S_j} r_0^{-1}[\mathbf{I} + \mathbf{R}(\mathbf{x}_0,\mathbf{y})]\, dS_y \tag{25}$$

$r_0 = |\mathbf{x}_0 - \mathbf{y}|$, where $\mathbf{x}_0$ is some point on the particle surface, and S_j and V_j denote particular surface and volume elements, respectively. In general, both $\mathbf{f}_j$ and $\mathbf{s}_j$ are unknown in eq 23. In the present work, however, where we are interested in the case of a polyion with fairly low surface potential interacting with a steady-state field, $\mathbf{e}(\mathbf{x})$, we can write

$$\mathbf{s}_j = \rho(\mathbf{x}_j)\mathbf{e}(\mathbf{x}_j) = qI(e^{-y(\mathbf{x}_j)} - e^{+y(\mathbf{x}_j)})\mathbf{e}(\mathbf{x}_j) \tag{26}$$

where q (=4.8 × 10^{-10} esu) is the electronic charge, I is the ionic strength (a single monovalent salt species is assumed), $y(\mathbf{x}_j)$ is the electrostatic potential in units of k_BT/q at $\mathbf{x}_j$ due to the polyion in the absence of an applied external field, and $\mathbf{x}_j$ is a point centrally located in volume element j. In turn, y represents the solution of the Poisson–Boltzmann equation which will depend on the specific details of the polyion and the amount of added salt. The case of a spherical polyion with a centrosymmetric charge distribution is discussed in a subsequent section.

Thus, only the $\mathbf{f}_j$ values in eq 23 are unknown. The details of the calculation of the surface and volume element integrations is given in the Appendix. Also, the work of Youngren and Acrivos[8] is recommended in this regard. Equation 23 represents a system of algebraic equations which can be solved by a number of matrix inversion or iterative techniques. In the present case, we have found Gauss–Seidel iteration to be a perfectly satisfactory method.[6] Multiply both sides of eq 23 by the inverse matrix, $\mathbf{C}_m^{-1}(\mathbf{x}_0)$, and rearrange to get

$$\mathbf{f}_m = \mathbf{C}_m^{-1}(\mathbf{x}_0)\cdot[-\mathbf{u} - \sum_{j=1}^{N}{}'\mathbf{C}_j(\mathbf{x}_0)\cdot\mathbf{f}_j - \sum_{j=N+1}^{M+N}\mathbf{B}_j(\mathbf{x}_0)\cdot\mathbf{s}_j] \tag{27}$$

where the prime on the first summation indicates exclusion of the $j = m$ term. Now in Gauss–Seidel iteration, one starts with an initial guess of the forces, $\mathbf{f}_m^{(1)}$, and sequentially updates each element using current estimates for the other terms. Thus, eq 27 becomes

$$\mathbf{f}_m^{(s+1)} = \mathbf{C}_m^{-1}(\mathbf{x}_0)\cdot[-\mathbf{u} - \sum_{j=1}^{m-1}\mathbf{C}_j(\mathbf{x}_0)\cdot\mathbf{f}_j^{(s+1)} - \sum_{j=m+1}^{N}\mathbf{C}_j(\mathbf{x}_0)\cdot\mathbf{f}_j^{(s)} - \sum_{j=N+1}^{M+N}\mathbf{B}_j(\mathbf{x}_0)\cdot\mathbf{s}_j] \tag{28}$$

where the s superscript refers to the iteration number. The procedure is repeated until the forces converge to some prespecified tolerance level, t, given by

$$t = [\sum_{j=1}^{N}(\mathbf{f}_j^{(s+1)} - \mathbf{f}_j^{(s)})^2 / \sum_{j=1}^{N}(\mathbf{f}_j^{(s+1)})^2]^{1/2} \tag{29}$$

In this work, we generally have set $t = 10^{-4}$ but the final results appear quite insensitive to this quantity in the range $10^{-2} > t > 10^{-6}$.

Once the $\mathbf{f}$'s have been determined, it is possible to compute fluid velocities and the pressure at any fluid point $\mathbf{x}$. From eqs 9–16 and the surface/volume decomposition scheme just discussed, it is straightforward to show

$$\mathbf{v}(\mathbf{x}) = \sum_{j=1}^{N}[\mathbf{a}_j(\mathbf{x}) + \mathbf{C}_j(\mathbf{x})\cdot\mathbf{f}_j] + \sum_{j=N+1}^{M}\mathbf{B}_j(\mathbf{x})\cdot\mathbf{s}_j \tag{30}$$

$$p(\mathbf{x}) = \sum_{j=1}^{N}[d_j(\mathbf{x}) + \mathbf{g}_j(\mathbf{x})\cdot\mathbf{f}_j] + \sum_{j=N+1}^{M}\mathbf{h}_j(\mathbf{x})\cdot\mathbf{s}_j \tag{31}$$

where

$$\mathbf{a}_j(\mathbf{x}) = \frac{3}{4\pi}\int\int_{S_j}\mathbf{r}r^{-3}[\mathbf{u}\cdot\mathbf{R}(\mathbf{x},\mathbf{y})\cdot\mathbf{n}(\mathbf{y})]\, dS_y \tag{32}$$

$$\mathbf{C}_j(\mathbf{x}) = \frac{1}{8\pi\eta}\int\int_{S_j} r^{-1}[\mathbf{I} + \mathbf{R}(\mathbf{x},\mathbf{y})]\, dS_y \tag{33}$$

$$\mathbf{B}_j(\mathbf{x}) = \frac{1}{8\pi\eta}\int\int\int_{V_j} r^{-1}[\mathbf{I} + \mathbf{R}(\mathbf{x},\mathbf{y})]\, d^3\mathbf{y} \tag{34}$$

$$d_j(\mathbf{x}) = -\frac{\eta}{2\pi}\int\int_{S_j} r^{-3}\mathbf{u}\cdot[\mathbf{I} - 3\mathbf{R}(\mathbf{x},\mathbf{y})]\cdot\mathbf{n}(\mathbf{y})\, dS_y \tag{35}$$

$$\mathbf{g}_j(\mathbf{x}) = \frac{1}{4\pi}\int\int_{S_j} r^{-3}\mathbf{r}\, dS_y \tag{36}$$

$$\mathbf{h}_j(\mathbf{x}) = \frac{1}{4\pi}\int\int\int_{V_j} r^{-3}\mathbf{r}\, d^3\mathbf{y} \tag{37}$$

Details regarding the calculation of eqs 32–37 are given in the Appendix.

Calculation of Electrophoretic Mobilities

The total hydrodynamic force on the polyion, $\mathbf{z}_H$, is

$$\mathbf{z}_H = -\sum_j \mathbf{f}_j A_j \tag{38}$$

where A_j is the area of the jth patch. Thus, $\mathbf{z}_H$ is readily calculated once the stress forces have been determined. In addition, there is an electrostatic force, $\mathbf{z}_E$, acting on the

polyion. Perhaps the most effective way to determine this quantity in general involves evaluation of the Maxwell stress tensor,[21,26] $\mathbf{T}(\mathbf{y})$, evaluated over the surface of the polyion, S_p.

$$\mathbf{z}_E = -\int\int_{S_p} \mathbf{T}(\mathbf{y})\cdot\mathbf{n}(\mathbf{y})\, dS_y \tag{39}$$

where $\mathbf{n}$ is the inward surface normal to the polyion

$$\mathbf{T}(\mathbf{y}) = \frac{\epsilon}{4\pi}\left[\mathbf{E}(\mathbf{y}) - \frac{1}{2}(\mathbf{e}(\mathbf{y})\cdot\mathbf{e}(\mathbf{y}))\mathbf{I}\right] \tag{40}$$

ϵ is the solvent dielectric constant, $\mathbf{e}(\mathbf{y})$ is the electric field at $\mathbf{y}$, and $E_{ij} = (\mathbf{e})_i(\mathbf{e})_j$ is the electric field dyadic. In evaluating $\mathbf{z}_E$ for model polyions in general, it may be inconvenient to evaluate eq 39 at the polyion–solvent interface because of discontinuities in dielectric constant or conductivity. From Gauss' law arguments, it can be shown that

$$-\int\int_{S_p} \mathbf{T}(\mathbf{y})\cdot\mathbf{n}(\mathbf{y})\, dS_y = -\int\int_{A} \mathbf{T}(\mathbf{y})\cdot\mathbf{n}(\mathbf{y})\, dS_y - \int\int\int_{V} \rho(\mathbf{y})\, \mathbf{e}(\mathbf{y})\, d^3\mathbf{y} \tag{41}$$

where A denotes some arbitrary closed surface which completely surrounds S_p, V is the intervening volume between S_p and A, and $\rho(\mathbf{y})$ denotes the solvent charge density.

The net force on the polyion is simply

$$\mathbf{z}_{Tot} = \mathbf{z}_H + \mathbf{z}_E \tag{42}$$

In a particular calculation, we do not know what the velocity of the polyion should be given that the applied field strength is $-\mathbf{e}_0$. Therefore, some initial estimate, $-\mathbf{u}_0$, is assumed (or $+\mathbf{u}_0$ if the polyion is negatively charged). Then $\mathbf{z}_H$ and $\mathbf{z}_E$ are calculated using the procedure discussed above. At this point, two approaches can be used to determine the actual velocity, $-\mathbf{u}$, of the polyion. The iterative method shall be discussed first. For a polyion in steady-state translation, $\mathbf{z}_{Tot}$ should vanish. If it does not, the calculation is repeated using a better estimate of the polyion velocity. In the present work, the assumption is made (incorrectly) that $\mathbf{z}_H$ scales linearly with the polyion velocity. That $\mathbf{u}$ is then chosen which is expected to yield a $\mathbf{z}_H$ which just balances $\mathbf{z}_E$. Although it might be expected that $\mathbf{z}_H$ would scale directly with $\mathbf{u}$, this is not the case. Even a polyion at rest in a fluid at rest subjected to an external field will have a nonvanishing $\mathbf{z}_H$. Physically, this is due to convection of counterions in the immediate vicinity of the polyion surface which, in turn, induces convective flow in the surrounding fluid. Because of this scaling problem, it is necessary to estimate $\mathbf{u}$ iteratively until $\mathbf{z}_{Tot}$ converges to zero. Once this has been achieved, the electrophoretic velocity, $-\mathbf{u}$, is determined. In the following section, we shall be reporting reduced mobilities, μ_{red}, defined by

$$\mu_{red} = \left(\frac{6\pi\eta q}{\epsilon k_B T}\right)\left(\frac{u}{e_0}\right) \tag{43}$$

A more efficient alternative is the method of O'Brien and White[17] which involves only two cycles. First, the polyion is translated with velocity $-\mathbf{u}_0$ in the absence of the electric field. Denote the resulting net force $\mathbf{z}_{Tot}^{(1)}$. In a second calculation, the polyion is held stationary in an external field, $-\mathbf{e}_0$, and $\mathbf{z}_{Tot}^{(2)}$ is determined. Provided the external field is small compared to the fields near the polyion, it is possible to simply superpose the solutions in the above two cases in such a way as to balance the forces to zero. If we write

$$\mathbf{z}_{Tot}^{(1)} = \alpha\mathbf{u}_0 \tag{44A}$$

then[17]

$$\mathbf{z}_{Tot}^{(2)} = \beta\mathbf{e}_0 \tag{44B}$$

$$u/e_0 = -\beta/\alpha \tag{45}$$

Both methods have been found to yield the same mobility within the uncertainty of the simulations, and the O'Brien and White approach is certainly the most efficient method. It should be stressed, however, that it is only valid at low external fields. It would not be appropriate, for example, to apply it to model studies of DNA fragments for fields of several kV/cm or higher.[27]

Application to a Sphere

In this section, the algorithm is applied to a nonconducting spherical polyion of radius a. The external electric field ($-\mathbf{e}_0$) and the reaction field of the polyion produce a net external field given by[13]

$$\mathbf{e}_{ext}(\mathbf{x}) = -\left(1 + \frac{a^3}{2x^3}\right)\mathbf{e}_0 + \frac{3a^3}{2x^5}(\mathbf{x}\cdot\mathbf{e}_0)\mathbf{x} \tag{46}$$

where $x = |\mathbf{x}|$. This is equivalent to the electric field outside a low dielectric sphere (dielectric constant = ϵ_{in}) in a high dielectric media (ϵ) in the limit $\epsilon \gg \epsilon_{in}$.[28] In order to calculate the external forces, $\mathbf{s}$, we also need charge densities following eq 3. Neglecting relaxation of the ion atmosphere due to $-\mathbf{e}_0$ (valid at low $\mathbf{e}_0$ and surface potential) and restricting ourselves to a single monovalent salt species

$$\rho(\mathbf{x}) = qI(e^{-y(\mathbf{x})} - e^{y(\mathbf{x})}) \tag{47}$$

where y is the reduced electrostatic potential (in units of k_BT/q) due to the polyion. Solution of the Poisson–Boltzmann equation yields y. Here y is approximated by simple but accurate Brenner–Roberts potentials[29] given by

$$y(\mathbf{x}) = y_{DH}(\mathbf{x})/(1 + a_3(y_0^3 - y_{DH}(\mathbf{x})^3)) \tag{48}$$

where

$$y_{DH} = y_0 a \exp(-\kappa(x - a))/x \tag{49}$$

$$a_3 = (1/Y - 1/y_0)/y_0^2 \tag{50}$$

y_0 is the reduced potential at $x = a$, $\kappa = 0.3293(I)^{1/2}$ Å^{-1} at 25 °C, and Y is a variational parameter described elsewhere.[29,30] In this work, we shall set $a = 20$ Å, $I = 0.576$ M (yielding $\kappa a = 5$), and $y_0 = 1$ and 5. The corresponding Y values turn out to be 0.988 and 3.697 for $y_0 = 1$ and 5, respectively. (In terms of polyion charges at this ionic strength, reduced surface potentials of 1 and 5 correspond to net charges of +17.32 and +171.88 given these Brenner–Roberts parameters.[30]) The no-salt ($I = 0$) case will also be studied to serve as an initial test of the algorithm.

The external forces are then given by

$$\mathbf{s}(\mathbf{x}) = qI(e^{-y(\mathbf{x})} - e^{+y(\mathbf{x})})\left(\mathbf{e}_{ext}(\mathbf{x}) - \frac{k_BT}{x}\frac{dy}{dx}\mathbf{x}\right) \tag{51}$$

The term involving the derivative dy/dx represents the external force on the fluid due to the polyion itself. It does not contribute to the mobility, total electrostatic force, or evidently the velocity field $\mathbf{v}(\mathbf{x})$ but is responsible for the osmotic pressure. It is straightforward to calculate the electrostatic force on the polyion by evaluating eqs 39 and 40 using the external field given by eq 46. (Again, the electric field due to the polyion itself does not contribute

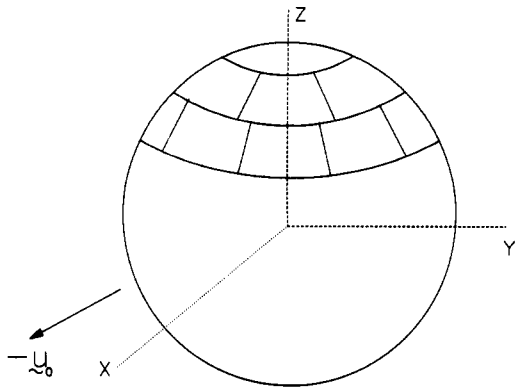

Figure 2. Surface of the spherical polyion subdivided into N patches of approximately equal area. The "polar patches" are chosen to lie along the z-axis of a local body fixed frame. Flow and field directions can be chosen arbitrarily.

Table I
Dependence of μ_{red} on Flow Direction and Patch Number (N) for $y_0 = 5$

N	flow direction	μ_{red}
44	x	5.90
44	y	5.93
44	z	7.58
44	av of above 3	6.47
44	magic angle[a]	6.47
168	x	6.00
168	y	6.03
168	z	6.76
168	av of above 3	6.26
168	magic angle[a]	6.27

[a] Flow direction along unit vector $(+3^{-1/2}, +3^{-1/2}, +3^{-1/2})$.

to $\mathbf{z}_E$.) It can be shown

$$\mathbf{z}_E = \epsilon a^2 \mathbf{e}_0 \frac{k_B T}{q} \left(\frac{dy}{dx}\right)_{x=a} \tag{52}$$

In the limit of zero salt, this simplifies to $\mathbf{z}_E = -Qq\mathbf{e}_0$ where Qq is the total polyion charge.

The surface of the sphere is subdivided into N patches of roughly equal area according to the following procedure. First, a variable number of latitudinal rings of constant angular extent, $\delta\theta$, are defined. The polar patches which result (chosen to lie along the $\pm z$ axis in a local body fixed frame of reference) are not subdivided any further. The areas of all remaining rings are greater than the polar patches. Consequently, they are subdivided into a number of equivalent units chosen in such a way that the areas are about the same as the polar patches. This is shown schematically in Figure 2. The number of patches (N) varies from 44 to 430 in this study which correspond to between 10 and 32 latitudinal divisions of the sphere. The M volume elements are chosen as follows. Between 20 and 250 spherical shells of thickness δr extend from the polyion surface ($r = a$) out to a distance where $y(r)/y_0$ falls to 10^{-3} or 10^{-4}. Each shell, in turn, is divided into N volume elements following the same procedure used to construct the surface patches.

In the absence of salt, the magnitude of the electrostatic and hydrodynamic forces are Qqe_0 and $6\pi\eta au$, respectively, and $\mu_{red} = Qq^2/\epsilon k_B T a$. Choosing the field and flow directions along z, we find that $\epsilon k_B T a \mu_{red}/Qq^2$ ranges from 1.016 to 1.008 as N is varied from 44 to 430. Thus, the alogorithm yields mobilities which converge to the correct limit in this limiting case. A more stringent test is to look at the stress forces, $\mathbf{f}_i$. In the absence of salt and for flow in the z direction, the actual stress forces should be $f_{ix} = f_{iy} = 0$ and $f_{iz} = -3\eta u/2a$ independent of patch position.

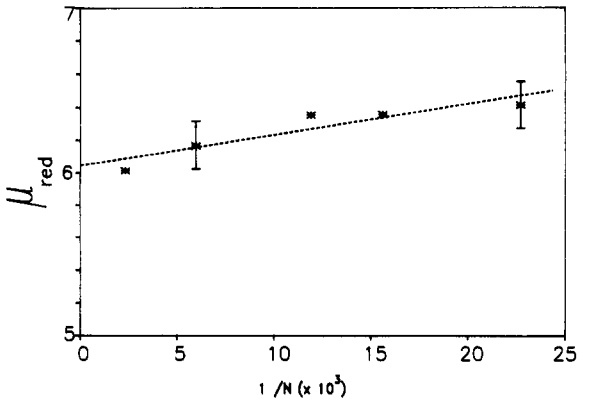

Figure 3. Dependence of μ_{red} on patch number (N) for $y_0 = 5$. Asterisks denote integral equation results.

Table II
Reduced Mobilities for Insulating Spheres with $\kappa a = 5$

y_0	μ_{red} (simulation)	μ_{red} (Henry)
1	1.22 ± 0.02	1.16
5	6.04 ± 0.12	6.07

In the integral equation approach, there is some variation in these forces. If, for example, we choose $\eta u/a = 1$, then the averages of the x, y, and z components come close to the expected values of 0, 0, and −1.5, respectively but the absolute standard deviations are about ±0.04 when N = 168. This variation is reduced by increasing N.

Turning now to studies with salt, the dependence of μ_{red} on flow or field direction will be considered first. (If we write $-\mathbf{u} = -u\mathbf{p}$ or $-\mathbf{e}_0 = -e_0\mathbf{p}$ where $\mathbf{p}$ is a unit vector, the flow/field direction is along $\mathbf{p}$.) Although the transport of a truly spherical particle should be independent of flow or field direction, partitioning the sphere into discrete patches breaks this symmetry to a limited extent. Shown in Table I are reduced mobilities for the case $y_0 = 5$ for $N = 44$ and 168 for different flow/field directions. There is clearly a significant dependence on flow direction but this decreases as N increases. Also note that mobilities obtained at the "magic angle" are in excellent agreement with the average of x, y, and z values. For this reason, all subsequent work is carried out at the magic angle. Reduced mobilities are insensitive to t (cutoff parameter), shell thickness (δr), and e_0 (magnitude of the applied field strength). A source of random error also enters because of the Monte Carlo method used to evaluate some of the volume integrals in eqs 24, 34, and 37. Briefly, the integrand is evaluated at a number of randomly selected points (typically 100) in the volume and the integral is approximated as the average times the volume of that element. Because of this, there is some variation in the final mobilities depending on the initial "seed" of the random number generator. Shown in Figure 3 is the reduced mobility for $y_0 = 5$ and variable N. The vertical bars reflect the random error discussed above and were obtained by carrying out five independent runs with different seeds. This error could be reduced by increasing the number of points in the Monte Carlo averaging procedure but was deemed unnecessary. From the least squares fit (dashed line) a reduced mobility of 6.04 ± 0.12 is obtained. This is in excellent agreement with μ_{red} = 6.07 predicted using Henry's equation.[13] For $y_0 = 1$, the variation of μ_{red} with N and the seed for the random number generator is substantially less than for $y_0 = 5$. The results are summarized in Table II. From this table, we can conclude that the alogorithm is yielding mobilities in good agreement with theoretical predictions subject to the starting assumptions of the model.

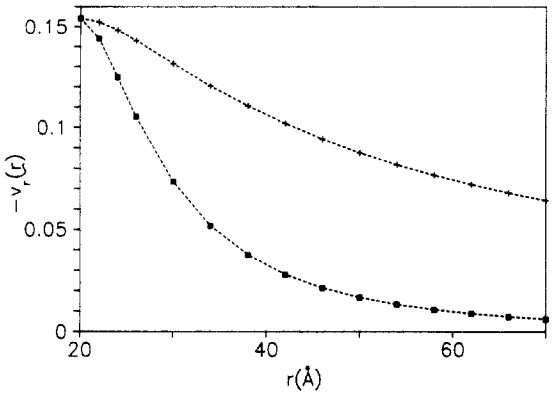

Figure 4. Effects of counterion atmosphere on $v_r(\mathbf{r})$ ($\theta = 0°$) for a 20-Å sphere. Squares denote the presence of salt with $y_0 = 1$, $\kappa a = 5$ ($I = 0.576$ M) and were computed using Henry's equations.[13] Crosses correspond to a sphere migrating with the same velocity, but in the absence of salt. Velocities are in cm/s.

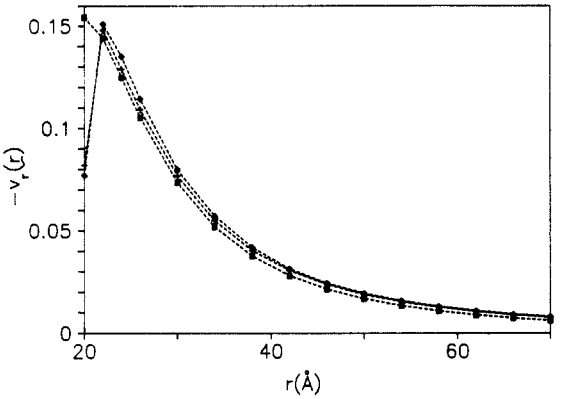

Figure 5. Henry (square) and DIE fields for $v_r(\mathbf{r})$ ($\theta = 0°$) for a 20-Å sphere with $y_0 = 1$, $\kappa a = 5$ ($I = 0.576$ M). Diamonds and crosses correspond to $N = 44$ and 430, respectively. Velocities are in cm/s.

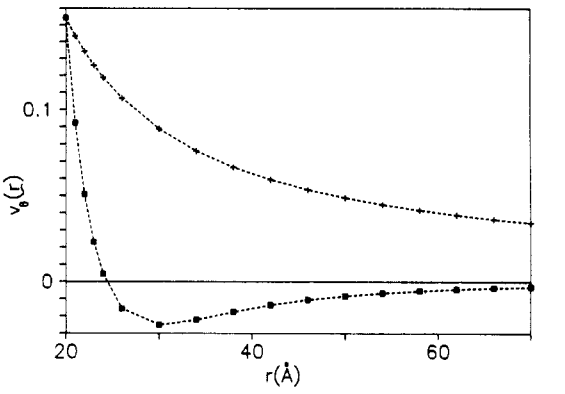

Figure 6. Similar to Figure 4, but $v_\theta(\mathbf{r})$ ($\theta = 90°$). Squares denote the presence of salt with $y_0 = 1$, $\kappa a = 5$ ($I = 0.576$ M) and were computed using Henry's equations.[13] Crosses correspond to a sphere migrating with the same velocity, but in the absence of salt. Velocities are in cm/s.

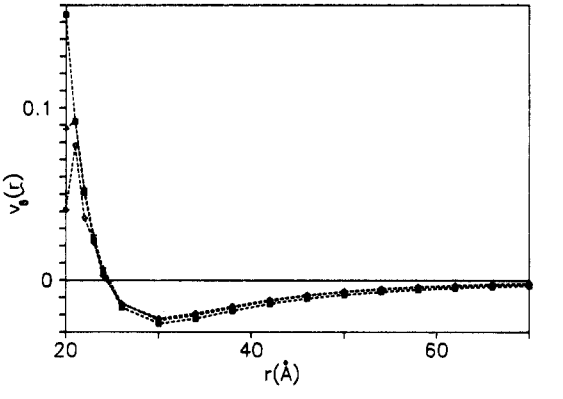

Figure 7. Henry (squares) and DIE fields for $v_\theta(\mathbf{r})$ ($\theta = 90°$) for a 20-Å sphere with $y_0 = 1$, $\kappa a = 5$ ($I = 0.576$ M). Diamonds and crosses correspond to $N = 44$ and 430, respectively. Velocities are in cm/s.

Early in the course of this work, Debye–Huckel potentials were also used ($Y = y_0$ in eqs 48–50). Debye–Huckel potentials are only a solution of Poisson's equation if linear terms in y are retained in eq 47 which relates the charge density to the electrostatic potential. Since Henry makes use of the Poisson equation in his derivation,[13] it is essential to use the linearized version of eq 47 in this case. Under these conditions, agreement between Henry and the integral equation approach is excellent.

Attention shall now be turned to the actual velocity and pressure profiles in the vicinity of the polyion calculated using eqs 30–37 for the DIE simulations and comparing them to the predictions of Henry.[13] In Figure 4, $-v_r(\mathbf{r})$, the radial component of $\mathbf{v}(\mathbf{r})$ in spherical coordinates, is plotted versus r for two cases using Henry's equations. In this case, $\theta = 0°$ where θ is measured relative to the "flow direction". (It should be kept in mind that the fluid velocity at the polyion surface is $-\mathbf{u} = -u\mathbf{p}$ where $\mathbf{p}$ denotes the "flow direction".) Squares correspond to a sphere with $a = 20$ Å, $y_0 = 1$, $I = 0.576$ M ($\kappa a = 5$), and $e_0 = 1$ kV/cm. Crosses correspond to a sphere translating at the same velocity but in the absence of salt (see p 124 of ref 29). Clearly, the presence of salt has a substantial effect on the velocity distribution. The corresponding profile for the DIE simulations are shown in Figure 5 for different patch numbers (N). The Henry profile (squares) is included for reference. It should be emphasized that the DIE velocities shown here were obtained by first balancing the electrostatic and hydrodynamic forces and only then calculating the velocity (and pressure) fields. In other words, the error in the polyion velocity is included here. As expected, agreement improves as N increases. However, even the crude $N = 44$ case agrees well with the actual distribution, except for r very close to a. This breakdown in the DIE velocities near the polyion–solvent interface is undoubtedly related to the discontinuity in the "double layer potential", $\mathbf{v}^{(2)}(\mathbf{x})$ mentioned under Integral Equations. In the case of the velocities, this should not pose any difficulties since surface values are known from the boundary conditions. Plotted in Figure 6 is $v_\theta(\mathbf{r})$ versus r for $\theta = 90°$. (This corresponds to the velocity component along $-\mathbf{p}$, but for field points on an axis perpendicular to $\mathbf{p}$.) As in Figure 4, squares represent the $y_0 = 1$, $I = 0.576$ M case predicted following Henry and crosses the corresponding no-salt limit. There is a simple physical explanation for the velocity profile when salt is present. Because of stick boundary conditions, the fluid velocity must approach the polyion velocity as r approaches a, so $v_\theta(\mathbf{r})$ will be positive. However, there will be a tendency of the counterion atmosphere to be pulled in the direction opposite that of the polyion. This produces convection of the solvent in a direction opposite to the polyions motion and hence the switch from positive to negative velocities. The ability of the DIE approach to reproduce this behavior is shown in Figure 7 for $N = 44$ (diamonds) and $N = 430$ (crosses). Except at $r \approx a$, agreement with the prediction of Henry is very good and improves as N increases.

Finally, pressure is considered in Figure 8 including the Henry distribution (squares). To emphasize that part of the field which depends on flow, the (dominant) osmotic pressure term has been subtracted out. The DIE results for $N = 168$ (diamonds) and $N = 430$ (crosses) evidently yield accurate pressures at large r though at $r \approx a$ agreement

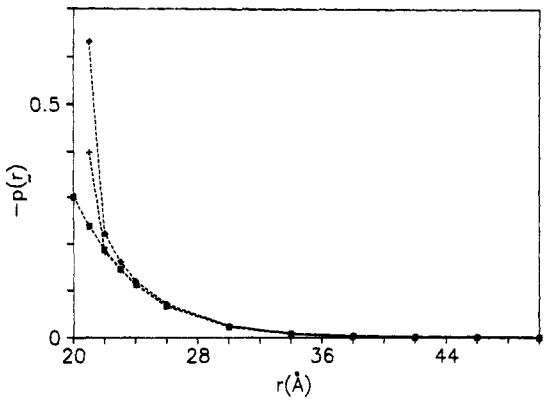

Figure 8. Pressure fields for a 20-Å sphere with $y_0 = 1$, $\kappa a = 5$ ($I = 0.576$ M) along the flow direction ($\theta = 0°$). The osmotic pressure has been subtracted out. Squares represent the predictions of Henry,[13] while diamonds and crosses are DIE results with $N = 168$ and 430, respectively. Pressures are in 10^{-11} dyn/Å^2.

breaks down. It is clear that the pressure field is more sensitive to N than the velocity field. For $N = 44$, for example, DIE pressures are very inaccurate and not included in the figure. Surface pressures will have to be estimated by extrapolation.

Summary

Because of the ubiquity of charged macromolecules, colloids, and micelles in nature, the whole problem of accounting for electrostatic effects is an extremely important one. One area in particular involves the transport of these species in an incompressible fluid. Although a great deal of theoretical work has been done on this problem for the case of the sphere and, to a lesser extent, the cylinder, much work remains to be done for a charged particle of arbitrary shape. Numerical methods offer a straightforward way of addressing this deficiency.

The main objectives of this work have been the extension of the DIE numerical method of Youngren and Acrivos[8] to include external forces and testing the alogorithm against a known standard. The "known standard" chosen is a charged spherical polyion and its associated ion atmosphere. The results of the previous section show that the algorithm yields accurate electrophoretic mobilities and is also able to reproduce the pressure and velocity fields around the polyion. The DIE computations presented here were carried out on a Silicon Graphics 4D/380 computer. CPU time to compute electrophoretic mobilities varies roughly as N^2. The $N = 44$ cases ran in about 1 min whereas the $N = 430$ cases required about 100 min. These timing runs were done using the iterative method of estimating the final electrophoretic mobility. It should also be kept in mind that calculating the pressure and velocity involves extensive computation at each fluid point. Although this is not time limiting for a small number of fluid points (up to about 100), it would become so for a large number.

In the near future, we will extend the present study in a number of respects. As shown by Wiersema and coworkers,[16] the external field induced relaxation of the ion atmosphere becomes important at high surface potentials, y_0. For a sphere with $\kappa a = 5$ (treated in this work), this relaxation becomes important for y_0 greater than about 2. Thus, relaxation in the case of our polyion with $y_0 = 1$ ($I = 0.576$ M, $a = 20$ Å, net polyion charge = 17.32) can be ignored but not the case with $y_0 = 5$ ($I = 0.576$ M, $a = 20$ Å, net polyion charge = 171.88). This relaxation complicates the problem since external forces are then no longer given by a simple Boltzmann distribution law (eq 47). Basically, what is required is a coupled solution of the Navier–Stokes and ion-transport equations.[15-17] We shall follow the strategy of using the DIE approach to first solve the Navier–Stokes equation for $\mathbf{v}(\mathbf{x})$ and $p(\mathbf{x})$ in the absence of relaxation; use these fields in solving the other equations by a finite difference method[31] to obtain corrected ion distributions; and then use these corrected ion distributions in the DIE algorithm to resolve the Navier–Stokes equation. This whole approach can be iterated. In addition to the relaxation problem, other geometries will also be considered, particularly the cylinder. Ultimately, we would like to apply it to the transport of DNA fragments of variable length.

Acknowledgment. We would like to acknowledge the donors of the Petroleum Research Fund, administered by the American Chemical Society, and a grant from the National Institutes of Health (GM46516-01) for partial support of this work.

Appendix

The surface and volume integrals appearing in eqs 24, 25, and 32–37 are evaluated in a number of ways depending on the distance, r, between source ($\mathbf{y}$) and field ($\mathbf{x}$) points. For surface integrals (with one notable exception discussed below) and volume integrals with average r values greater than some cutoff distance σ (chosen to be 20 Å in this work), the surface/volume element is broken down into 16 or 25 domains of comparable area/volume. The integral is approximated as the sum of the product of the area/volume of the domain times the value of the integrand evaluated at a point in the center of the domain. Varying the number of domains was found to have a negligible effect on the final mobilities but obviously has a large effect on computational time.

For volume elements with $r < \sigma$, a number (typically 100) of points within the volume are selected entirely at random and the average of the integrand is evaluated. The integral is approximated as the product of the integrand average times the volume of the element. This Monte Carlo procedure introduces random error into the problem, but the magnitude of this error can be assessed by carrying out several runs with different seeds for the random number generator. This point is discussed in the text.

Equation 25 is solved analytically when $\mathbf{x}_0$ lies inside S_j. Consider the case of a small spherical patch with surface outward normal in the $+z$ direction and $\mathbf{x}_0$ located at its center. Generalization to nonspherical patches and/or patches with their normal not along $+z$ will be carried out later. If the radius of curvature is a and its angular extent (from the z-axis) $\delta\theta$, then it is straightforward to show

$$\mathbf{C}_j^0 = A_j^{1/2} \begin{pmatrix} \frac{3}{8\eta\pi^{1/2}} & 0 & 0 \\ 0 & \frac{3}{8\eta\pi^{1/2}} & 0 \\ 0 & 0 & \frac{1}{4\eta\pi^{1/2}} \end{pmatrix} \quad \text{(A1)}$$

where $A_j = \pi a^2 \delta\theta^2$ is the circular patch area and the zero superscript denotes that the patch normal is along the $+z$ axis of our body-fixed coordinate system. Youngren and Acrivos considered a more general surface integral over a *square* patch.[8] Applying their eqs B3–B8 to a square patch with $\mathbf{x}_0$ and the patch normal along $+z$ yields a matrix

equivalent to eq A1 to three significant figures. Thus, we conclude eq A1 can be applied to other patch shapes as well.

The corresponding matrices for elements not along $+z$ can be evaluated using the properties of cartesian matrices undergoing a rotational transformation of the coordinate system.[32] Let θ and ϕ be the polar and azimuthal angle the outward normal makes with respect to your body-fixed coordinate system. Then

$$\mathbf{C}_j = \mathbf{Q}^T \mathbf{C}_j^0 \mathbf{Q} \tag{A2}$$

where

$$\mathbf{Q} = \begin{pmatrix} \cos\theta\cos\phi & \cos\theta\sin\phi & -\sin\theta \\ -\sin\phi & \cos\phi & 0 \\ \sin\theta\cos\phi & \sin\theta\sin\phi & \cos\theta \end{pmatrix} \tag{A3}$$

References and Notes

(1) Bloomfield, V. A.; Dalton, W. O.; van Holde, K. E. *Biopolymers* **1967**, *5*, 135.
(2) McCammon, J. A.; Deutch, J. M. *Biopolymers* **1976**, *15*, 1397.
(3) Garcia de la Torre, J.; Bloomfield, V. A. *Biopolymers* **1977**, *16*, 1747, 1765.
(4) Nakajima, H.; Wada, Y. *Biopolymers* **1977**, *16*, 875.
(5) Teller, D. C.; Swanson, E.; de Haen, C. *J. Chem. Phys.* **1980**, *72*, 1623.
(6) Garcia de la Torre, J.; Bloomfield, V. A. *Q. Rev. Biophys.* **1981**, *14*, 81.
(7) Ladyzhenskaya, O. A. *The Mathematical Theory of Viscous Incompressible Flow*; Gordon and Breach: New York, 1963; Chapter 3.
(8) Youngren, G. K.; Acrivos, A. *J. Fluid. Mech.* **1975**, *69*, 377.
(9) Youngren, G. K.; Acrivos, A. *J. Chem. Phys.* **1975**, *63*, 3846.
(10) Loeb, A. L.; Overbeek, J. Th. G.; Wiersema, P. H. *The Electric Double Layer Around a Spherical Colloid Particle*; MIT Press: Cambridge, MA, 1961.
(11) Hunter, R. J. *Zeta Potentials in Colloid Science*; Academic Press: New York, 1981.
(12) von Smoluchowski, M. *Bull. Acad. Sci. Cracovie* **1903**, 182.
(13) Henry, D. C. *Proc. R. Soc. London* **1931**, *A133*, 106.
(14) Overbeek, J. Th. G. *Adv. Colloid Sci.* **1950**, *3*, 97.
(15) Booth, F. *Proc. R. Soc. London* **1950**, *A203*, 514.
(16) Wiersema, P. H.; Loeb, A. L.; Overbeek, J. Th. G. *J. Colloid Interface Sci.* **1966**, *22*, 78.
(17) O'Brien, R. W.; White, L. R. *J. Chem. Soc., Faraday Trans 2* **1978**, *74*, 1607.
(18) O'Brien, R. W.; Hunter, R. J. *Can. J. Chem.* **1981**, *59*, 1878.
(19) Oshima, H.; Healy, T. W.; White, L. R. *J. Chem. Soc., Faraday Trans. 2* **1983**, *79*, 1613.
(20) Stigter, D. *J. Phys. Chem.* **1978**, *82*, 1417, 1424.
(21) Fixman, M. *J. Chem. Phys.* **1980**, *72*, 5177.
(22) Fixman, M. *Macromolecules* **1980**, *13*, 711.
(23) Derjaguin, B. V.; Dukhin, S. S.; Shilov, V. N. *Adv. Colloid Interface Sci.* **1980**, *13*, 141.
(24) Dukhin, S. S.; Shilov, V. N. *Adv. Colloid Interface Sci.* **1980**, *13*, 153.
(25) Happel, J.; Brenner, H. *Low Reynolds Number Hydrodynamics*; Martinus Nijhoff: The Hague, Netherlands, 1983.
(26) Landau, L. D.; Lifshitz, E. M. *Electrodynamics of Continuous Media*; Pergamon Press: London, 1960.
(27) Rau, D. C.; Charney, E. *Macromolecules* **1983**, *16*, 1653.
(28) Jackson, J. D. *Classical Electrodynamics*; Wiley: New York, 1975.
(29) Brenner, S. L.; Roberts, R. E. *J. Phys. Chem.* **1973**, *77*, 2367.
(30) Allison, S. A.; Sines, J. J.; Wierzbicki, A. *J. Phys. Chem.* **1989**, *93*, 5819.
(31) Warwicker, J.; Watson, H. C. *J. Mol. Biol.* **1982**, *157*, 671.
(32) Arfken, G. *Mathematical Methods for Physicists*; Academic Press: New York, 1970.